applied sciences

MDPI

Communication

Thermodynamic Simulations for Determining the Recycling Path of a Spent Lead-Acid Battery Electrolyte Sample with $Ca(OH)_2$

Shuai Gu [1], Bitian Fu [2], Toyohisa Fujita [3] and Ji Whan Ahn [1,*]

1 Center for Carbon Mineralization, Mineral Resources Division, Korea Institute of Geoscience and Mineral Resources, 124 Gwahak-ro, Gajeong-dong, Yuseong-gu, Daejeon 34132, Korea; gushuai@kigam.re.kr
2 Shanghai Environment Sanitation Engineering Design and Research Institute Co. Ltd., Shanghai 200232, China; bitianfu@hotmail.com
3 School of Resources, Environment, and Materials, Guangxi University, 100 Daxue Rd, Nanning 530004, China; fujitatoyohisa@gxu.edu.cn
* Correspondence: ahnjw@kigam.re.kr

Received: 9 May 2019; Accepted: 27 May 2019; Published: 31 May 2019

Featured Application: This thermodynamic simulation can help design the recycling process of spent lead-acid battery electrolyte. The effect of ambient CO_2 and pH can be simulated by thermodynamic calculations.

Abstract: By utilizing thermodynamic calculations, the possible removal path of spent lead-acid battery electrolytes was modeled. The process was divided into precipitation and carbonation processes. In the carbonation process, two scenarios were discussed, namely carbonation with and without pre-filtration of the precipitates resulted from the precipitation process. The results showed that in the precipitation process, the theoretical limit for the chemical removal of SO_4^{2-} was 99.15%, while in the following carbonation process without filtration, only 69.61% of SO_4^{2-} was removed due to the fact that CO_2 reacts with Ca^{2+} ion in the solution, and thus leads to the production of $CaCO_3$ and SO_4^{2-} ions in the solution. In the carbonation process without filtration, with the increase of CO_2 in the solution the removal ratio of SO_4^{2-} further decreases. Thermodynamic simulation was effective in predicting the theoretical removal limits and helps in understanding and optimizing the removal process.

Keywords: thermodynamic simulations; spent lead-acid battery; electrolyte; carbonation

1. Introduction

Lead-acid batteries (LAB) are widely used in motor vehicles [1,2], backup power supplies [3], and stand-alone power systems [4,5] due to their properties of excellent reliability, low cost, good operation life, high surge currents, and relatively large power-to-weight ratio [6]. LABs, as the single most-used battery system worldwide, consume approximately 85% of the total global lead production [7]. To satisfy the huge and ever-increasing demand for lead worldwide, in 2014 alone 2.46 million tons of secondary lead was recovered from spent LABs. [8] The first step in the recycling process is disassembly, in which spent LABs are separated into four parts, i.e., the grid, with the main composition being lead (92~95%), lead paste, which is mainly composed of lead oxide (PbO), lead dioxide (PbO_2), lead sulfate ($PbSO_4$), and lead (Pb) plastics, which are the main composition of shells, and electrolytes, with the main composition being sulfate acid (38 wt.% H_2SO_4). The grid separated from spent LABs is commonly refined for utilization in the manufacture of new LABs [9]. The lead paste has been intensively studied with various hydrometallurgy and pyrometallurgy

techniques [10–14]; shells are also recovered as polypropylene for manufacturing new LABs [15,16], and the electrolytes are normally collected for further purification [8]. However, in spent LAB recycling plants, installation of new devices is required to collect and handle the highly corrosive electrolytes. In a typical disassembly and refinery plant, spent electrolytes are often discharged onto the ground and collect in a pit, which makes the purification process unreasonable for recycling. The typical recycling methods of SO_4^{2-} ions from wastewater include: adsorption [17], chemical precipitation [18,19], biological treatment [20], and ion exchange [21]. Due to the high concentrations of SO_4^{2-} in the spent electrolytes, chemical precipitation was adopted. $BaCl_2$ [22], limestone [19], and ettringite [23] have been used to remove SO_4^{2-} in wastewater, while no detailed theoretical calculation has been reported. In this paper, the systematic theoretical calculations of spent LAB electrolytes' reactions with $Ca(OH)_2$ were conducted, and sulfate ions were then recovered as $CaSO_4{\cdot}2H_2O$. Thermodynamic calculations were utilized to simulate the whole process, based on which the optimum conditions and recycling path were obtained. The thermodynamic simulation predicted the theoretical chemical precipitation removal efficiency and suggested that ambient CO_2 should be avoided in the precipitation process and filtration should be adopted before the carbonation process to achieve higher efficiency.

2. Materials and Methods

2.1. Materials

The spent LAB electrolyte sample was received from Dansuk Industrial Co., Ltd., Gyeonggi-do, Korea. The spent electrolyte sample was first filtered and analyzed with Inductively coupled plasma-optical emission spectrometry (ICP-OES) to measure the concentration of SO_4^{2-} ions. The concentration of SO_4^{2-} in the spent electrolyte was 147,000 mg/L. The main impurities of the spent electrolyte were Ca^{2+}, Mg^{2+}, and Pb^{2+} (3.01 mg/L). Due to the low concentrations of both Ca^{2+} and Mg^{2+} and the fact that both ions are not toxic, only Pb^{2+} was discussed in detail in this research. The pH of the spent electrolyte solution was measured with a Thermo Scientific™ Orion™ Versa Star Pro™ pH meter equipped with a highly sensitive ROSS Ultra 8302BNUMD electrode, with the mean pH being −0.53.

2.2. Methods

The thermodynamic calculations were carried out with Matlab® R2010a software using thermodynamic parameters of all possible reactions. At the first stage, spent H_2SO_4 from the electrolyte sample was precipitated with $Ca(OH)_2$ powder until the solution was almost saturated calcium hydroxide, then the carbonation processes were simulated, both with and without pre-filtration of the precipitates resulted from the precipitation process. All simulations were performed under the condition that the temperature was kept at 25 °C at all times. Equations (1)–(3), (4)–(13), and (14)–(21) from Table 1 were used in the calculation of the thermodynamic equilibrium distributions of the saturated solutions of $Ca(OH)_2$, $CaCO_3$, and $CaSO_4{\cdot}2H_2O$, respectively, while Equations (21)–(29) and (30)–(43) from Table 1 were utilized to calculate the thermodynamic distributions of different species during the precipitation process and carbonation process after filtration of the precipitates. Equations (44)–(47), together with Equations (23), (24), (26)–(29), (34), (35), (37), and (39) from Table 1, were utilized to calculate the carbonation process without the filtration of precipitates resulted from the precipitation process. Equations (48)–(55) and (56)–(61) from Table 1 were used to calculate the thermodynamic distributions of Pb^{2+} in precipitation and carbonation processes, respectively. All species (aqueous species and precipitates) at different pH can be obtained by solving the matrix of equilibrium constants and mass balances.

It is worth pointing out that in the modeling process of carbonation, the system was considered as a closed system with a certain amount of CO_2 injected into the system. This was adopted due to the fact that CO_2 was the gas and the amount of CO_2 consumed cannot be easily obtained.

Due to the fact that calcium, sulfate, and carbonate are all divalent ions with quite low ionic activity coefficients (γ), which are $\gamma_{Ca^{2+}}$ = 0.28 (I = 0.7, 25 °C and 1 atm), $\gamma_{SO_4^{2-}}$ = 0.12, and $\gamma_{CO_3^{2-}}$ = 0.20 (I = 0.7, 25 °C and 1 atm), respectively, the activity corrections are needed in the thermodynamic modeling process. The definition of ionic strength (I) and activity coefficient are shown in Equations (1) and (2) [24]:

$$I = 1/2 \sum m_i Z_i^2 \tag{1}$$

$$\gamma_i = \frac{a_i}{m_i} \tag{2}$$

where m_i is the molality of an aqueous species, i is the corresponding aqueous species, Z_i is the charge of i, a_i is activity of species i, and γ_i is the activity coefficient of species i. In this study, a simplified Helgeson-Kirkham-Flowers model was used to calculate the activity coefficient, as shown in Equation (3) [25–27]:

$$Log\gamma_i = -AZ_i^2\left(\sqrt{\frac{I}{1+B\sqrt{I}}}\right) - Log\left(1 + 0.018\sum m_k\right) + bI \tag{3}$$

where A is the Debye-Hückel slope, B is the distance of the closest approach, b is a solute specific parameter, and k is all solute species in the aqueous solution.

3. Results

3.1. Precipitation

Figure 1 shows the thermodynamic calculations of 30 mM $Ca(OH)_2$ in aqueous solution at 25 °C with different pH. The theoretical values were obtained by solving the matrix consisting of both equilibrium constants (Equations (2) and (3) from Table 1) and mass balances (Equations (4) and (5)). With Matlab, this set of equations were simultaneously solved with 100 steps in the whole pH range (0~14), thus giving the distribution of each species at different pH. In the case of $Ca(OH)_2$ solution, four species, Ca^{2+}, $CaOH^+$, OH^-, and $Ca(OH)_2$(s), were taken into consideration. Figure 1a shows the log concentrations of different species in 30 mM $Ca(OH)_2$ solution with different pH. Log concentrations were adopted due to the low concentrations of each species. As can be seen, with the increase of pH the concentration of Ca^{2+} first stays unchanged when pH < 12.6, while with the further increase of pH, the concentration of Ca^{2+} decreased slowly, and at the same time $Ca(OH)_2$(s) emerged in the solution as a precipitate. $CaOH^+$ ions started to appear at pH 6, the log concentration of which increased linearly until pH 12.6, after which the log concentration of $CaOH^+$ ions started to decrease linearly. In Figure 1b, the fraction of calcium was calculated vs. pH, and a similar change of concentration was also observed for Ca^{2+}, $CaOH^+$, and $Ca(OH)_2$. The theoretical parameters of saturated $Ca(OH)_2$ are shown in Table 1; as can be seen, the theoretical pH of saturated $Ca(OH)_2$ is 12.45 with $C_{Ca^{2+}}$ = 19.48 mM. Similarly, the equilibrium distributions of saturated $CaCO_3$ solution can be calculated by solving the matrix composed of Equations (4)–(13) from Table 1 (thermodynamic parameters) and (6)–(8) (mass balances). The distributions of different species in $CaCO_3$ solution was also shown in Figure 2 and Table 1. As can be seen, for the saturated solution of $CaCO_3$, the equilibrium pH is 9.94 and $C_{Ca^{2+}}$ = 0.1415 mM. For the saturated $CaCO_3$ solution, if the pH is high enough (pH > 13), Ca^{2+} from $CaCO_3$(s) will dissolve into solution and form $Ca(OH)_2$(s), thus causing the increase of concentration of free Ca^{2+} ions. As for saturated $CaSO_4$ solution (Figure 3), the equilibrium pH is 7.08 and the equilibrium $C_{Ca^{2+}}$ = 12.03 mM. In the saturated solution of $CaSO_4$, the main precipitate would be $CaSO_4{\cdot}2H_2O$; as can be seen from Figure 3b, with the increase of pH $CaSO_4{\cdot}2H_2O$ starts to decrease at pH 11 and the dominant precipitate becomes $Ca(OH)_2$(s) at approximately pH 13. Therefore, for recovering $CaSO_4{\cdot}2H_2O$, the pH should be controlled properly. By comparing the data in Figures 1 and 2, it is clear that the equilibrium concentration of Ca^{2+} in $CaCO_3$ solution was significantly smaller than that in $Ca(OH)_2$ solution, which was caused by the much smaller solubility products (K_{sp}) of $CaCO_3$, and should carbonation

happen in the precipitation process the concentration of Ca^{2+} should also decrease, which would, in turn, cause the increase of SO_4^{2-}. Based on the results obtained from Figures 1–3, we conclude that the saturated $CaCO_3$ solution has the lowest equilibrium $C_{Ca^{2+}}$, and contacting with CO_2 might decrease the concentration of Ca^{2+} ions, which will help us better understand the carbonation process discussed in Section 3.2. The detailed species distribution of saturated $Ca(OH)_2$, $CaCO_3$ and $CaSO_4$ can be found in Table 2.

Table 1. Chemicals, formulas, reactions, and equilibrium constants used in the thermodynamic calculations.

Formulas	Possible Chemical Reactions		$Log_{10}(K)$ [1]
H^+/OH^-	$H_2O \leftrightarrow H^+ + OH^-$	(1)	−13.99
Ca^{2+}	$2H^+ + Ca(OH)_2(s) \leftrightarrow Ca^{2+} + 2H_2O$	(2)	22.62
$CaOH^+$	$H^+ + Ca(OH)_2(s) \leftrightarrow CaOH^+ + H_2O$	(3)	9.785
$Ca(OH)_2(s)$	$CaCO_3(s) + 2H_2O \leftrightarrow 2H^+ + 2CO_3^{2-} + Ca(OH)_2(s)$	(4)	−30.88
$CaO(s)$	$CaCO_3(s) + H_2O \leftrightarrow 2H^+ + 2CO_3^{2-} + CaO(s)$	(5)	−41.0
$CaCO_3$	$CaCO_3(s) \leftrightarrow CaCO_3$	(6)	−4.961
$CaHCO_3^+$	$CaCO_3(s) + H^+ \leftrightarrow CaHCO_3^+$	(7)	3.08
$CaOH^+$	$CaCO_3(s) + H_2O \leftrightarrow H^+ + 2CO_3^{2-} + CaOH^+$	(8)	−21.11
CO_2	$2H^+ + CO_3^{2-} \leftrightarrow H_2O + CO_2$	(9)	16.68
$CO_2(g)$	$2H^+ + CO_3^{2-} \leftrightarrow H_2O + CO_2(g)$	(10)	18.15
H_2CO_3	$2H^+ + CO_3^{2-} \leftrightarrow H_2CO_3$	(11)	16.70
HCO_3^-	$H^+ + CO_3^{2-} \leftrightarrow HCO_3^-$	(12)	10.33
Ca^{2+}	$CaCO_3(s) \leftrightarrow Ca^{2+} + CO_3^{2-}$	(13)	−8.30
$CaOH^+$	$CaSO_4(s) + H_2O \leftrightarrow CaOH^+ + H^+ + SO_4^{2-}$	(14)	−17.21
$CaSO_4$	$CaSO_4(s) \leftrightarrow CaSO_4$	(15)	−2.190
Ca^{2+}/SO_4^{2-}	$CaSO_4(s) \leftrightarrow Ca^{2+} + SO_4^{2-}$	(16)	−4.378
$Ca(OH)_2$ (s)	$CaSO_4(s) + 2H_2O \leftrightarrow Ca(OH)_2(s) + 2H^+ + SO_4^{2-}$	(17)	−26.99
$CaO(s)$	$CaSO_4(s) + H_2O \leftrightarrow CaO + 2H^+ + SO_4^{2-}$	(18)	−37.08
$CaSO_4{\cdot}2H_2O$ (s)	$CaSO_4(s) + 2H_2O \leftrightarrow CaSO_4{\cdot}2H_2O(s)$	(19)	0.161
H_2SO_4	$2H^+ + SO_4^{2-} \leftrightarrow H_2SO_4$	(20)	0.780
HSO_4^-	$H^+ + SO_4^{2-} \leftrightarrow HSO_4^-$	(21)	1.982
$CaOH^+$	$Ca(OH)_2(s) + H^+ \leftrightarrow H_2O + CaOH^+$	(22)	9.785
$CaSO_4$	$CaSO_4{\cdot}2H_2O(s) \leftrightarrow CaSO_4 + 2H_2O$	(23)	−2.351
Ca^{2+}	$Ca(OH)_2(s) + 2H^+ \leftrightarrow Ca^{2+} + 2H_2O$	(24)	22.62
$CaO(s)$	$Ca(OH)_2(s) \leftrightarrow CaO(s) + H_2O$	(25)	−10.09
$CaSO_4(s)$	$CaSO_4{\cdot}2H_2O(s) \leftrightarrow CaSO_4(s) + 2H_2O$	(26)	−0.161
H_2SO_4	$CaSO_4{\cdot}2H_2O(s) \leftrightarrow H_2SO_4 + Ca(OH)_2(s)$	(27)	−26.37
HSO_4^-	$CaSO_4{\cdot}2H_2O(s) \leftrightarrow HSO_4^- + Ca(OH)_2(s) + H^+$	(28)	−25.17
SO_4^{2-}	$CaSO_4{\cdot}2H_2O(s) \leftrightarrow SO_4^{2-} + Ca(OH)_2(s) + 2H^+$	(29)	−13.99
$CaCO_3$	$Ca^{2+} + CO_2 + H_2O \leftrightarrow CaCO_3 + 2H^+$	(30)	22.62
$CaHCO_3^+$	$Ca^{2+} + CO_2 + H_2O \leftrightarrow CaHCO_3^+ + H^+$	(31)	9.785
$CaOH^+$	$Ca^{2+} + H_2O \leftrightarrow CaOH^+ + H^+$	(32)	−30.88
$CaSO_4$	$Ca^{2+} + SO_4^{2-} \leftrightarrow CaSO_4$	(33)	−41.0
$CO_2(g)$	$CO_2 \leftrightarrow CO_2(g)$	(34)	−4.961
H_2CO_3	$CO_2 + H_2O \leftrightarrow H_2CO_3$	(35)	3.080
H_2SO_4	$2H^+ + SO_4^{2-} \leftrightarrow H_2SO_4$	(36)	−21.11
HCO_3^-	$CO_2 + H_2O \leftrightarrow H^+ + HCO_3^-$	(37)	16.68
HSO_4^-	$H^+ + SO_4^{2-} \leftrightarrow HSO_4^-$	(38)	18.15
CO_3^{2-}	$CO_2 + H_2O \leftrightarrow 2H^+ + CO_3^{2-}$	(39)	16.7
$Ca(OH)_2(s)$	$Ca^{2+} + 2H_2O \leftrightarrow Ca(OH)_2(s) + 2H^+$	(40)	10.33
$CaCO_3(s)$	$Ca^{2+} + 2H_2O + CO_2 \leftrightarrow CaCO_3(s)$	(41)	−8.30
$CaSO_4(s)$	$Ca^{2+} + SO_4^{2-} \leftrightarrow CaSO_4(s)$	(42)	−17.21
$CaSO_4{\cdot}2H_2O(s)$	$Ca^{2+} + SO_4^{2-} + 2H_2O \leftrightarrow CaSO_4{\cdot}2H_2O$ (s)	(43)	−2.19
$CaCO_3$	$Ca(OH)_2(s) + CO_2 \leftrightarrow CaCO_3 + H_2O$	(44)	−4.378
$CaHCO_3^+$	$Ca(OH)_2(s) + CO_2 + H^+ \leftrightarrow CaHCO_3^+ + H_2O$	(45)	−26.99
$CaOH^+$	$Ca(OH)_2(s) + H^+ \leftrightarrow CaOH^+ + H_2O$	(46)	−37.08
$CaCO_3(s)$	$Ca(OH)_2(s) + CO_2 \leftrightarrow CaCO_3(s) + H_2O$	(47)	0.161
$Pb(OH)_2$	$Pb^{2+} + 2H_2O \leftrightarrow Pb(OH)_2 + 2H^+$	(48)	−17.12
$Pb(OH)_3^-$	$Pb^{2+} + 3H_2O \leftrightarrow Pb(OH)_3^- + 3H^+$	(49)	−28.06

Table 1. *Cont.*

$Pb_3(OH)_4^{2+}$	$2Pb2+ + 4H_2O \leftrightarrow Pb_3(OH)_4^{2+} + 4\,H^+$	(50)	−23.88
$PbOH^+$	$Pb^{2+} + H_2O \leftrightarrow PbOH^+ + H^+$	(51)	−7.71
$PbSO_4$	$Pb^{2+} + SO_4^{2-} \leftrightarrow PbSO_4$	(52)	2.69
$Pb(OH)_2(s)$	$Pb^{2+} + 2H_2O \leftrightarrow Pb(OH)_2(s) + 2H^+$	(53)	−13.6
$PbO(s)$	$Pb^{2+} + 2H_2O \leftrightarrow PbO(s) + 2H^+$	(54)	−12.9
$PbSO_4(s)$	$Pb^{2+} + SO_4^{2-} \leftrightarrow PbSO_4(s)$	(55)	7.79
$Pb(CO_3)_2^{2-}$	$Pb^{2+} + 2H_2O + 2CO_2 \leftrightarrow Pb(CO_3)_2^{2-} + 4H^+$	(56)	−23.26
$PbCO_3$	$Pb^{2+} + H_2O + CO_2 \leftrightarrow PbCO_3 + 2H^+$	(57)	−10.08
$PbCO_3OH^-$	$Pb^{2+} + 2H_2O + 2CO_2 \leftrightarrow PbCO_3OH^- + 3H^+$	(58)	−18.48
$PbHCO_3^+$	$Pb^{2+} + H_2O + CO_2 \leftrightarrow PbHCO_3^+ + H^+$	(59)	−3.331
$Pb_3(CO_3)_2(OH)_2(s)$	$3Pb^{2+} + 3H_2O + 2CO_2 \leftrightarrow Pb_3(CO_3)_2(OH)_2(s) + 6H^+$	(60)	−13.96
$PbCO_3(s)$	$Pb^{2+} + H_2O + CO_2 \leftrightarrow PbCO_3(s) + 2H^+$	(61)	−3.48

Note: [1.] *K* data obtained from HSC Chemistry® 6.0 database.

$$C_{Ca^{2+}} + C_{Ca(OH)_2(s)} + C_{CaOH^+} = Ca_{total} \tag{4}$$

$$2 \times C_{Ca^{2+}} + C_{CaOH^+} = C_{OH^-} \tag{5}$$

$$C_{CaCO_3(s)} + C_{CaCO_3} + C_{CaHCO_3} + C_{Ca^{2+}} = C_{Ca_{total}} \tag{6}$$

$$C_{CaCO_3(s)} + C_{CaCO_3} + C_{CaHCO_3} + C_{CO_3^{2-}} + C_{HCO_3^-} + C_{H_2CO_3} + C_{CO_2} + C_{CO_2(g)} = C_{CO_3^{2-}\,total} \tag{7}$$

$$C_{CaHCO_3} + C_{HCO_3^-} + 2 \times \left(C_{H_2CO_3} + C_{CO_2} + C_{CO_2(g)}\right) = C_{OH^-} \tag{8}$$

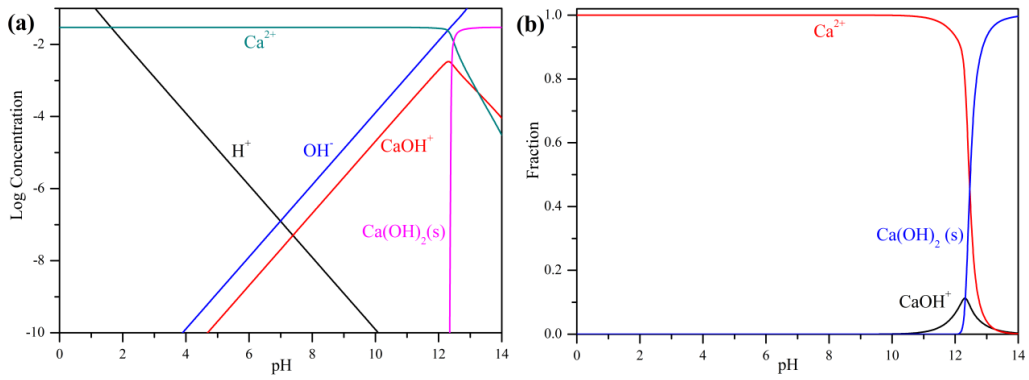

Figure 1. Calculated species distributions of 30 mM $Ca(OH)_2$ at different pH: (**a**) with log concentration vs. pH; (**b**) with fraction of calcium vs. pH.

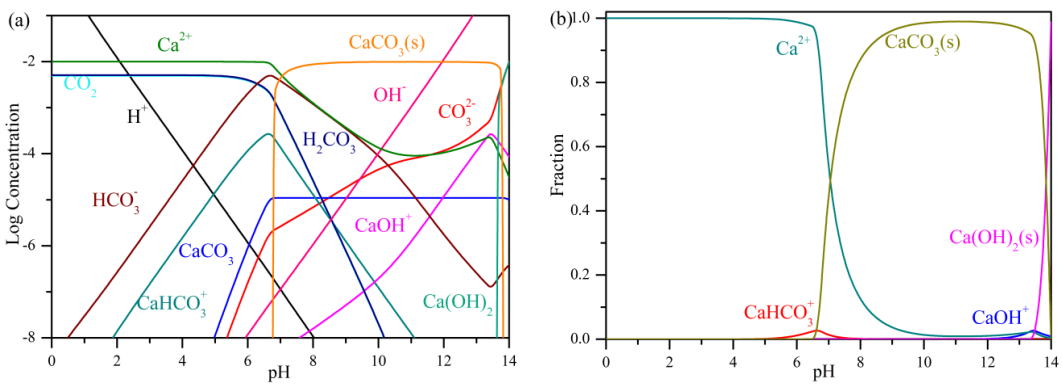

Figure 2. Calculated species distributions of 10 mM $CaCO_3$ at different pH: (**a**) with log concentration vs. pH; (**b**) with fraction of calcium vs. pH.

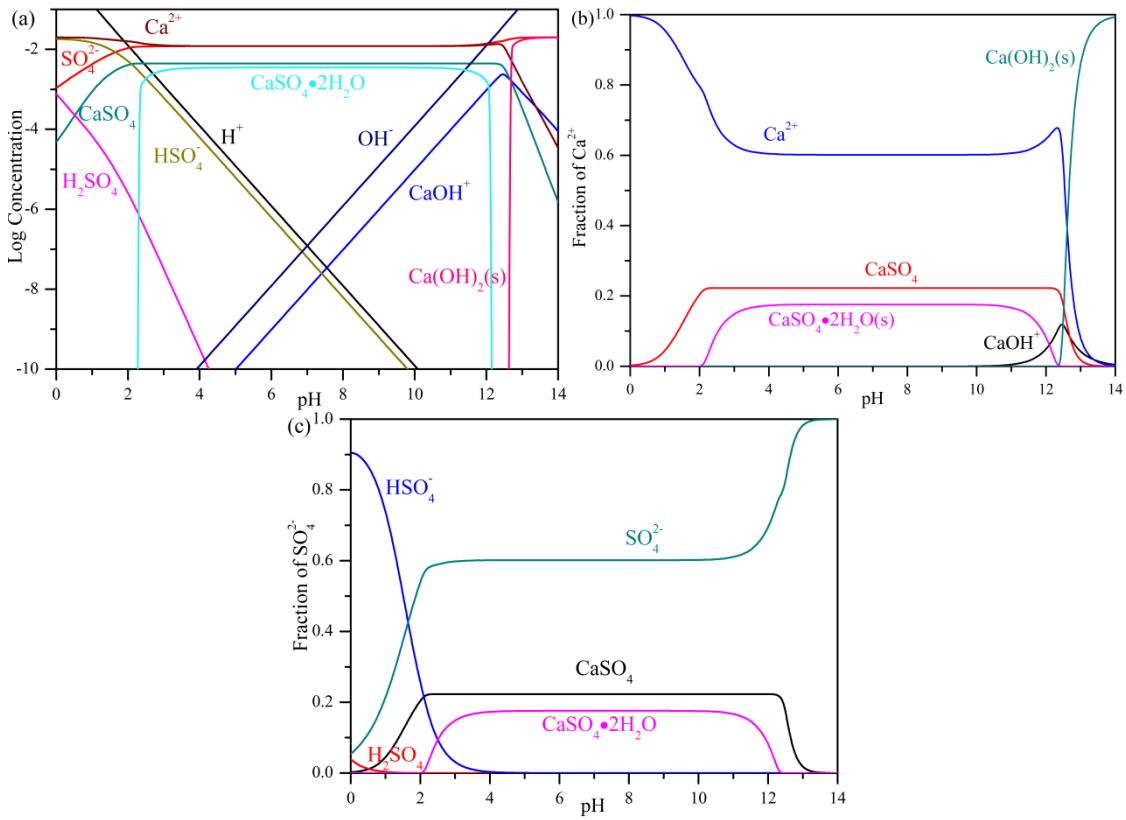

Figure 3. Calculated species distributions of 20 mM $CaSO_4$ at different pH: (**a**) with log concentration vs. pH; (**b**) with fraction of calcium vs. pH; (**c**) with fraction of sulfate vs. pH.

Table 2. Calculated concentrations of different species in saturated $Ca(OH)_2$, $CaCO_3$, and $CaSO_4$ solutions.

Contents	Species	Concentrations (mM)
Saturated $Ca(OH)_2$ (30 mM)	$Ca(OH)_2$ (s)	7.203
	Ca^{2+}	19.48
	OH^-	28.44
	$CaOH^+$	3.318
Saturated $CaCO_3$ (10 mM)	$CaCO_3$(s)	9.847
	$CaCO_3$	1.094×10^{-2}
	$CaHCO_3^+$	1.415×10^{-4}
	OH^-	8.886×10^{-2}
	Ca^{2+}	0.1415
	CO_3^{2-}	4.318×10^{-2}
	HCO_3^-	9.840×10^{-2}
	H_2CO_3	2.560×10^{-5}
	CO_2	2.468×10^{-5}
Saturated $CaSO_4$ (20 mM)	OH^-	1.212×10^{-4}
	SO_4^{2-}	12.03
	$CaOH^+$	9.681×10^{-6}
	$CaSO_4$	4.457
	H_2SO_4	3.236×10^{-13}
	HSO_4^-	6.279×10^{-5}
	Ca^{2+}	12.03
	$CaSO_4{\cdot}2H_2O$	3.516

According to the ICP-OES measurement results, the concentration of SO_4^{2-} in the spent electrolyte sample was 1.53 M. Figure 4 shows the reaction equilibriums of 1.53 M SO_4^{2-} reacting with 1.55 M

$Ca(OH)_2$ at different pH. Extra $Ca(OH)_2$ was introduced to ensure the removal of SO_4^{2-} ions. As can be seen from Figure 4, the main precipitates were $CaSO_4{\cdot}2H_2O$ in a wide pH range (pH: 2~12), according to Equation (9), and when pH < 2 [19], $CaSO_4{\cdot}2H_2O$ would dissolve into the solution and become Ca^{2+} and SO_4^{2-} ions, according to Equation (10). At the same time, if pH > 12, the ratio of $CaSO_4{\cdot}2H_2O$ might also decrease because of the formation of $Ca(OH)_2(s)$ (Figure 4c) and SO_4^{2-} (Figure 4b), according to Equation (11). The final pH and composition of the mixture are shown in Table 3; as can be seen, the equilibrium pH of the mixture is 12.42 with $C_{Ca^{2+}}$ = 25.06 mM, $C_{SO_4^{2-}}$ = 8.668 mM, and $C_{CaSO4{\cdot}2H2O}$ = 1517 mM. Based on these data, the removal ratio of SO_4^{2-} can be calculated and shown in Table 3. Also, by comparing the data obtained from the precipitation process with the saturated $CaCO_3$ and $CaSO_4$ solution data, the result indicates that if CO_2 was introduced in the precipitation process, the removal efficiency of SO_4^{2-} might decrease. Therefore, ambient CO_2 should be avoided in the precipitation process to obtain a higher removal efficiency. Also, the theoretical results obtained in this model are very close to the experimental results of Fang et al. [23].

$$Ca(OH)_2(s) + H_2SO_4 \leftrightarrow CaSO_4{\cdot}2H_2O\ (s) \tag{9}$$

$$CaSO_4{\cdot}2H_2O\ (s) + H^+ \leftrightarrow HSO_4^- + Ca^{2+} + 2H_2O \tag{10}$$

$$CaSO_4{\cdot}2H_2O\ (s) + 2OH^- \leftrightarrow Ca(OH)_2(s) + SO_4^{2-} + 2H_2O \tag{11}$$

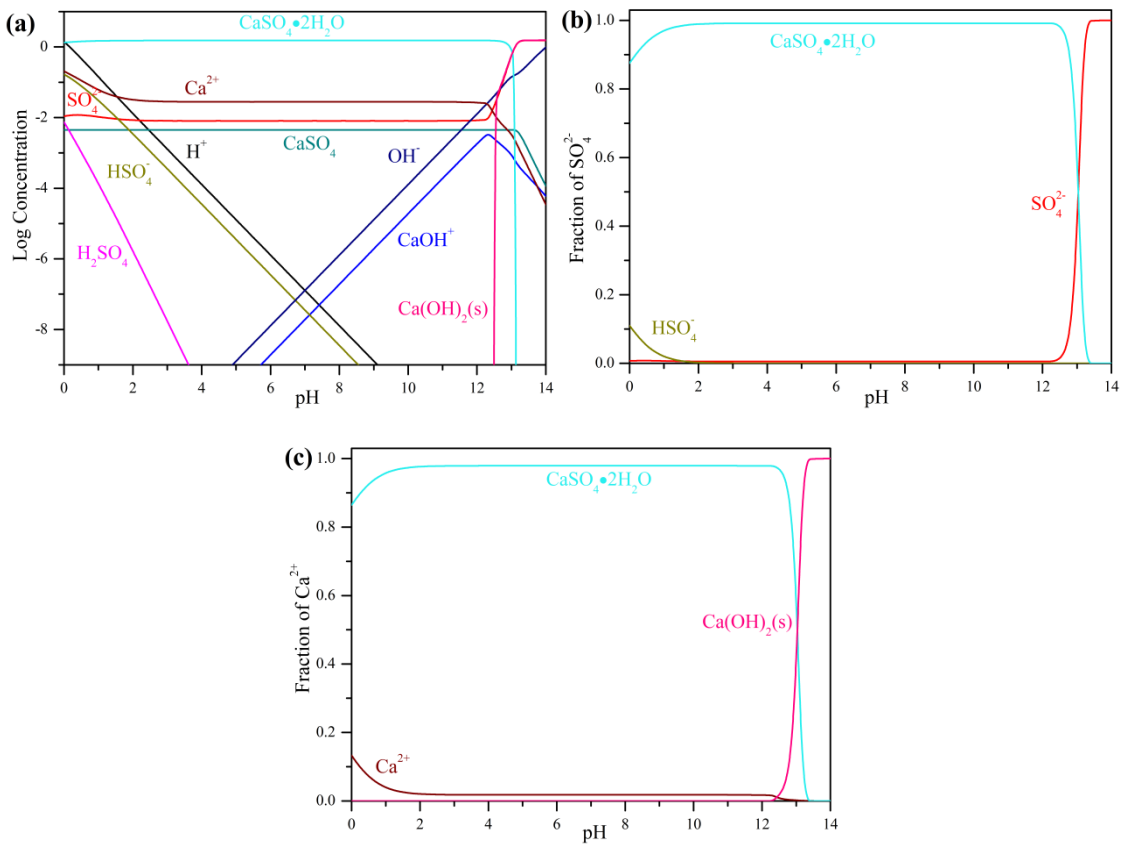

Figure 4. Calculated species distributions of 1.53 M SO_4^{2-} reacting with 1.55 M $Ca(OH)_2$ at different pH: (**a**) with log concentration vs. pH; (**b**) with fraction of sulfate vs. pH; (**c**) with fraction of calcium vs. pH.

Table 3. Calculated equilibrium species distributions of the precipitation process and carbonation process, with and without filtration.

Contents	Species	Concentrations (mM)	Removal Efficiency of SO_4^{2-}/Pb^{2+}
1.55 M $Ca(OH)_2$ + 1.53 M SO_4^{2-}	OH^-	26.53	99.15%
	$CaOH^+$	3.605	
	$CaSO_4$	4.457	
	Ca^{2+}	25.06	
	SO_4^{2-}	8.668	
	$CaSO_4{\cdot}2H_2O$	1517	
	$Pb(OH)_2$	3.447×10^{-4}	0
	$Pb(OH)_3^-$	1.416×10^{-2}	
Carbonation after filtration at pH 7 (0.1 M CO_2)	Ca^{2+}	0.4509	99.15%
	SO_4^{2-}	13.01	
	$CaSO_4$	0.1118	
	HCO_3^-	57.32	
	$CaCO_3(s)$	32.44	
	$PbCO_3(s)$	1.397×10^{-2}	96.35%
	$PbCO_3$	2.512×10^{-4}	
	$PbHCO_3^+$	1.834×10^{-4}	
	$Pb(CO_3)_2^{2-}$	7.332×10^{-5}	
Carbonation without filtration at pH 7 (0.1 M CO_2)	$CaSO_4$	4.457	69.61%
	HCO_3^-	20.48	
	Ca^{2+}	4.098	
	SO_4^{2-}	460.43	
	$CaCO_3(s)$	476.2	
	$CaSO_4{\cdot}2H_2O$	1065	

Figure 5 shows the distributions of lead-related ions at different pH. As can be seen from Figure 5a, no precipitation was formed in the whole pH range due to the extremely low concentration of lead and the existence of SO_4^{2-} (Table 3). [28] This might be in favor of the precipitation process due to the fact that lead is toxic, and according to this simulation, no lead was precipitated in the precipitation process with $Ca(OH)_2$. Figure 5b shows the fraction of lead at different pH, based on which the distribution of lead can be divided into three regions: at low pH region (pH < 2), the main form of lead is Pd^{2+}; at moderate pH region (2 < pH < 7), lead was mainly in the form of $PbSO_4$ (Equation (52) from Table 1); at high pH region (pH > 7), lead forms a complex with OH^- ions and forms four kinds of complexes with the increase of pH (Equations (48)–(51) from Table 1).

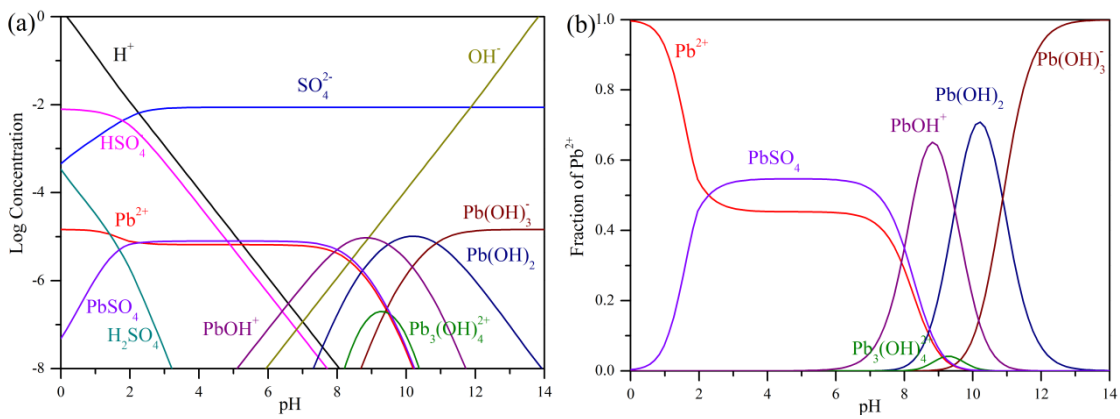

Figure 5. Calculated species distributions of 8.67 mM SO_4^{2-} reacting with 0.0145 mM Pb^{2+} at different pH: (**a**) with log concentration vs. pH; (**b**) with fraction of lead vs. pH.

3.2. Carbonation

After the precipitation process, the extra $Ca(OH)_2$ should be removed and the carbonation process introduced to both remove extra $Ca(OH)_2$ and neutralize the solution. Due to the fact that the appearance of CO_2 might promote the production of $CaCO_3$, which in turn might influence the final products of the carbonation process, the carbonation process was divided into 2 scenarios: with filtration and without filtration of the precipitates resulted from the precipitation process, respectively. In the filtration and carbonation scenario, the total calcium concentration (T_{Ca}) $T_{Ca} = C_{Ca^{2+}} + C_{CaOH+} + C_{CaSO4} = 33.122$ mM, while the total sulfate concentration ($T_{SO4}{}^{2-}$) $T_{SO4}{}^{2-} = C_{SO4}{}^{2-} + C_{CaSO4} = 13.125$ mM. Figure 6 shows the calculated species distributions of the carbonation process after filtration; as can be seen, the main precipitate when pH > 6 was $CaCO_3$ (Equation (12)), while in the pH range of 3~5 the main precipitate was $CaSO_4{\cdot}2H_2O$ (Equation (43) from Table 1). As shown in Figure 6b, with the increase of pH the ratio of calcium in Ca^{2+} ion form decreases and the ratio in $CaCO_3$ form increases, which was caused by the formation of $CaCO_3$ in the alkaline region (Equation (12)). As can be seen from Figure 6c, when the pH > 7, the dominant species is $SO_4{}^{2-}$, because the dissociation of $CaSO_4$ (Equation (13)) and the dissociation of $CaSO_4$ were caused by the constant removal of Ca^{2+} according to Equation (12). When the final pH is 7, the equilibrium species distributions are shown in Table 3; as can be seen, the equilibrium $C_{[Ca^{2+}]} = 0.4509$ mM, $C_{[SO_4{}^{2-}]} = 13.01$ mM, and the main precipitate was $CaCO_3$(s) (32.44 mM).

$$Ca^{2+} + CO_2 + 2OH^- \leftrightarrow CaCO_3(s) + H_2O \quad (12)$$

$$CaSO_4 \leftrightarrow Ca^{2+} + SO_4{}^{2-} \quad (13)$$

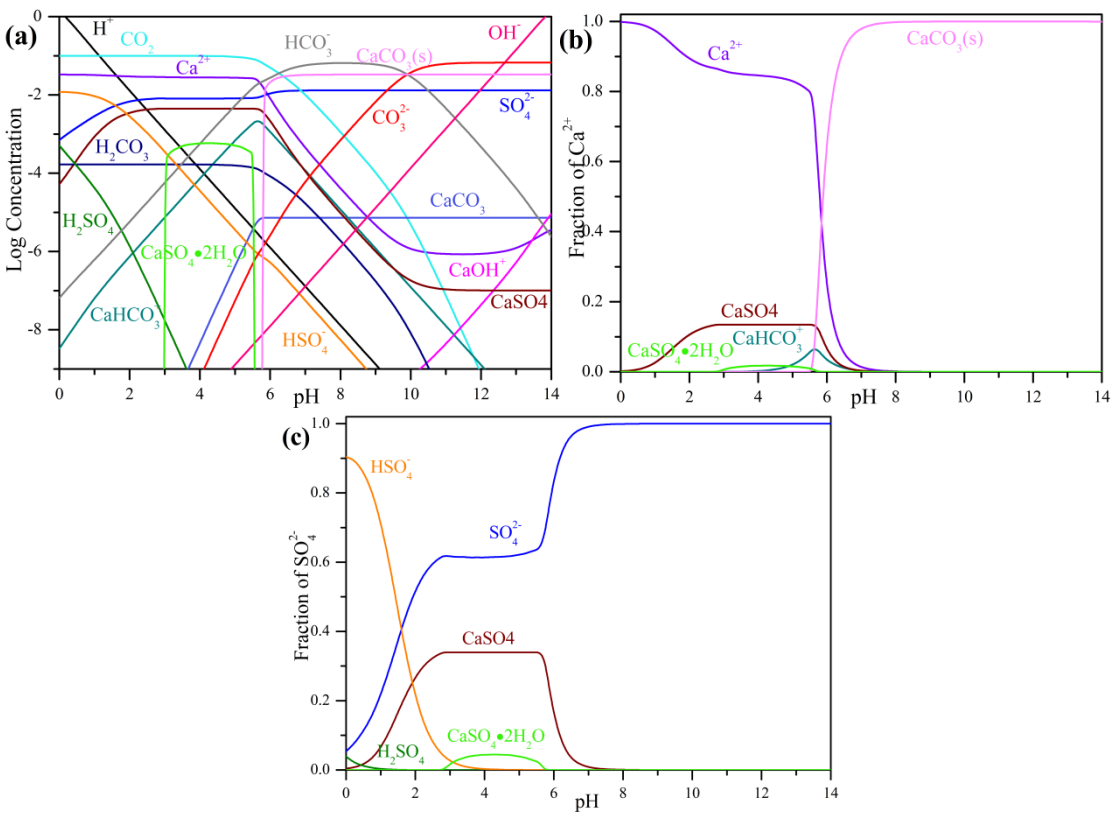

Figure 6. Calculated species distributions of carbonation process with filtration at different pH: (**a**) with log concentration vs. pH; (**b**) with fraction of calcium vs. pH; and (**c**) with fraction of sulfate vs. pH.

In the case of carbonation without filtration, the total calcium concentration is $T_{ca} = 1.55$ M, and the total sulfate concentration is $T_{SO4^{2-}} = 1.53$ M. As can be seen from Figure 7, the dominant precipitated

species were $CaSO_4{\cdot}2H_2O$ (pH: 2~5, Equation (9)), $CaSO_4{\cdot}2H_2O$ and $CaCO_3$ (pH: 5~13, Equations (9) and (12)), and $Ca(OH)_2(s)$ and $CaCO_3$ (pH: 13~14, Equations (11) and (12)), respectively. When pH is smaller than 2, a certain amount of $CaSO_4{\cdot}2H_2O$ would dissolve, as can be seen from Figure 7b (Equation (10)). The decrease of $C_{CaSO4{\cdot}2H2O}$ in pH 5–7 was mainly caused by the formation of $CaCO_3$ (Equation (12)), which leads to the dissolution of $CaSO_4{\cdot}2H_2O$ (Equation (14)), and simultaneously results in the increase of $C_{SO_4^{2-}}$ in the same region. In other words, this decrease of $C_{CaSO4{\cdot}2H2O}$ in pH 5–7 resulted from the combination of $CaSO_4{\cdot}2H_2O$ dissolution reactions (Equation (14)) and carbonation reaction (Equation (12)). When pH is larger than 13, the fraction of $CaSO_4{\cdot}2H_2O$ further decreases to almost zero; this was caused by both the formation of $CaCO_3$ (Equation (12)), and most importantly, the formation of $Ca(OH)_2(s)$ (Equation (11)) at extremely high pH. The fraction of $CaSO_4{\cdot}2H_2O$ decreases with the increase of CO_2 concentrations, according to Figure 7b–d. To obtain a higher removal ratio of SO_4^{2-}, 0.1 M CO_2 was chosen. The equilibrium species distributions of the solution at pH 7 are listed in Table 3; the equilibrium $C_{Ca^{2+}}$ = 4.098 mM, $C_{SO_4^{2-}}$ = 460.43 mM, $C_{CaCO3(s)}$ = 476.2 mM, and $C_{CaSO4{\cdot}2H2O}$ = 1065 mM. The calculated removal ratio of sulfate, in this case, is lower (69.61%) than the carbonation after filtration (99.15%).

$$CaSO_4{\cdot}2H_2O\ (s) \leftrightarrow Ca^{2+} + SO_4^{2-} + 2H_2O \tag{14}$$

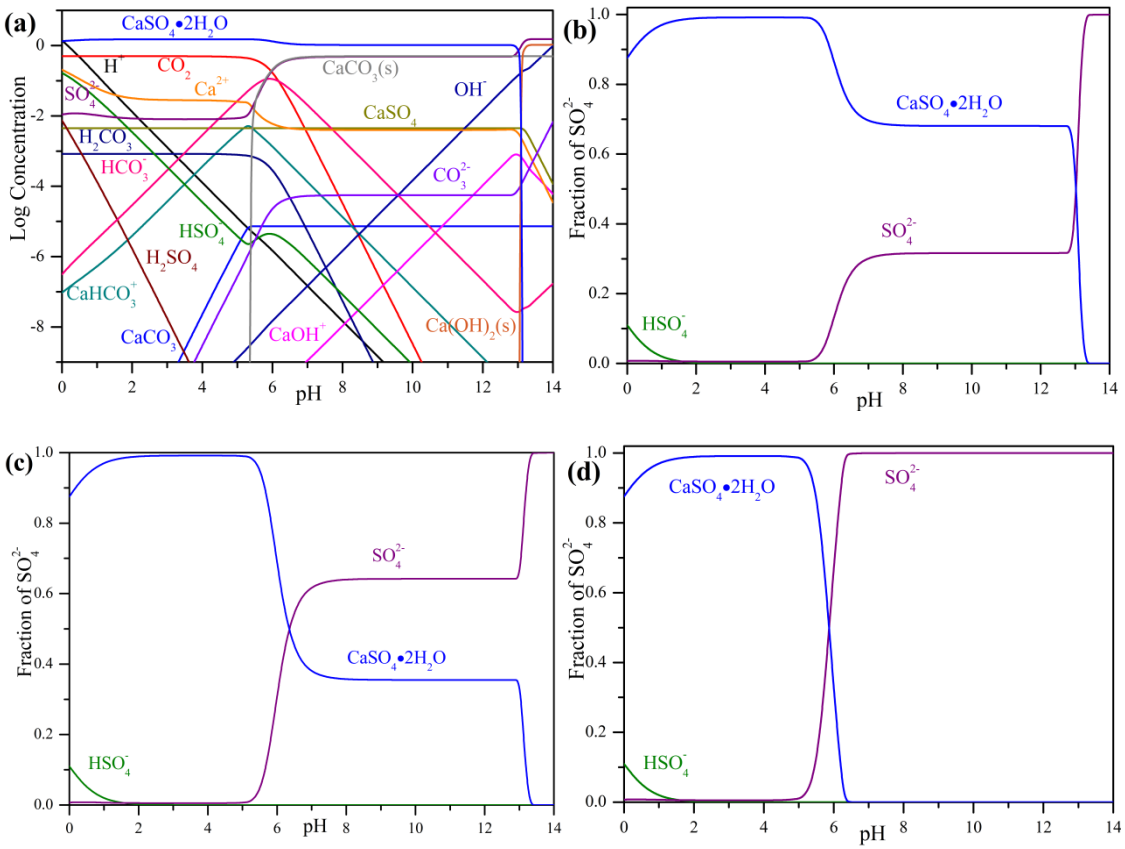

Figure 7. Calculated species distributions of carbonation process without filtration at different pH: (**a**) C_{CO_2} = 0.1 M with log concentration vs. pH; (**b**) C_{CO_2} = 0.1 M with fraction of sulfate vs. pH; (**c**) C_{CO_2} = 1 M with fraction of sulfate vs. pH; and (**d**) C_{CO_2} = 2 M with fraction of sulfate vs. pH.

Since carbonation with filtration was a better option than carbonation without filtration, only carbonation with filtration was calculated for lead (Figure 8). As can be seen from Figure 8a, the $PbCO_3(s)$ precipitate (Equation (61) from Table 1) existed in the moderate pH region (5 < pH < 9); when pH is lower than this value $PbCO_3(s)$ might react with H^+ to form $PbHCO_3^+$, according to

Equation (15), while at a higher pH with the increase of pH, $PbCO_3(s)$ might react with both CO_3^{2-} and OH^- to form $Pb_3(CO_3)_2OH_2(s)$ (Equation (16)), $Pb(CO_3)_2^{2-}$ (Equation (17)), $PbCO_3OH^-$ (Equation (18)), and $Pb(OH)_3^-$ (Equation (19)), respectively. The end pH = 7 was adopted for the carbonation process, in which 96.35% of lead was precipitated as $PbCO_3(s)$, and thus stabilized with $CaCO_3$ in the carbonation process (Table 3).

$$PbCO_3(s) + H^+ \leftrightarrow PbHCO_3^+ \quad (15)$$

$$3PbCO_3(s) + 2OH^- \leftrightarrow Pb_3(CO_3)_2OH_2(s) + CO_3^{2-} \quad (16)$$

$$PbCO_3(s) + CO_3^{2-} \leftrightarrow Pb(CO_3)_2^{2-} \quad (17)$$

$$PbCO_3(s) + OH^- \leftrightarrow PbCO_3OH^- \quad (18)$$

$$PbCO_3(s) + 3OH^- \leftrightarrow Pb(OH)_3^- + CO_3^{2-} \quad (19)$$

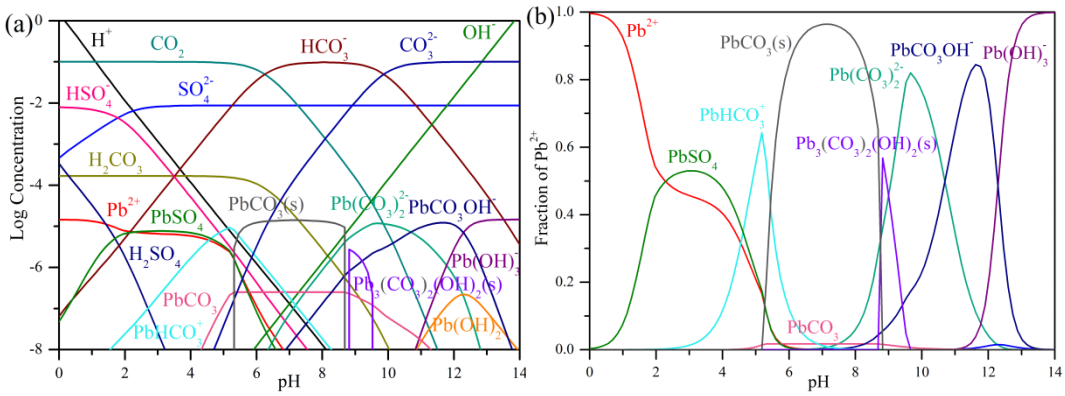

Figure 8. Calculated lead related species distributions of carbonation process with filtration at different pH: (**a**) C_{CO_2} = 0.1 M with log concentration vs. pH; and (**b**) C_{CO_2} = 0.1 M with fraction of lead vs. pH.

4. Conclusions

Normally, the spent LAB electrolytes can be directly filtered and reused on the condition that the electrolytes were collected and handled properly in the dissembling plant. For dissembling plants without appropriate collecting setups, electrolytes are often polluted with foreign ions, since electrolytes are often discharged onto the ground directly. These polluted electrolytes cannot be purified by simple filtration, and thus require more reasonable recycling techniques. Instead, it is more reasonable and profitable to recycle and stabilize SO_4^{2-} in the form of $CaSO_4{\cdot}2H_2O$, which can be widely used as a fertilizer and for building materials. In this study, the polluted electrolyte sample was recycled with chemical precipitation and carbonation techniques. To understand the whole recycling process, thermodynamic simulations in the precipitation and carbonation processes were conducted. The thermodynamic calculations of saturated $Ca(OH)_2$, $CaCO_3$, and $CaSO_4$ solutions helped us to understand the whole process, since $Ca(OH)_2$ and $CaSO_4$ appear in both precipitation and carbonation processes when the pH is higher than 13. Additionally, $CaCO_3$ appears in the carbonation process with and without filtration. The theoretical limit for the removal ratio of SO_4^{2-} was predicted to be 99.15% with 1.53 M SO_4^{2-} and 1.55 M $Ca(OH)_2$. Also, by comparing the carbonation process with and without pre-filtration of the precipitates obtained from the precipitation process, the theoretical removal efficiency of SO_4^{2-} was calculated to be 99.15% and 69.61%, respectively. With the increase of CO_2 concentrations in the solution, the removal efficiency of SO_4^{2-} further decreased. Furthermore, the chemical precipitation and carbonation of lead in the spent electrolyte sample were calculated; no precipitation existed in the precipitation process due to the appearance of SO_4^{2-}, while 96.35% of lead was precipitated as $PbCO_3(s)$ in the carbonation process, which stabilized lead with $CaCO_3$. The thermodynamic calculations helped us to design and understanding the whole removal process quantitatively. Based on the thermodynamic calculation results, the optimized removal process of

SO_4^{2-} should be precipitation without contact with ambient CO_2, since $PbCO_3$ might precipitate around pH 9, which would lead to the existence of lead in $CaSO_4{\cdot}2H_2O$. Additionally, filtration should be undertaken before the carbonation process to avoid the re-dissolution of $CaSO_4{\cdot}2H_2O$. After filtration, the final product of the recycling process ($CaSO_4{\cdot}2H_2O$) is obtained. In the following carbonation process, the flow rate of CO_2 and pH should be controlled properly to stabilize lead and extra calcium in the form of $PbCO_3$ and $CaCO_3$, respectively. At last, after chemical precipitation and carbonation, there is still around 13 mM SO_4^{2-} in the solution, which needs to be removed by adsorption or ion-exchange techniques. The overall theoretical chemical precipitation limit for removal of SO_4^{2-} was 99.15%. The limitation of the simulation was: (1) in the simulation process of carbonation, where the system was assumed to be a closed system with all CO_2 dissolved in the solution; and (2) equilibrium at each pH is achieved by both carbonation reaction and addition of HCl or NaOH when needed. These limitations might cause the deviation of simulation values from experimental results, however, the tendency of the whole process should be similar, which makes the simulation of the carbonation process a good tool for reference.

Author Contributions: Conceptualization, T.F. and J.W.A.; data curation, B.F.; formal analysis, B.F.; investigation, S.G.; methodology, S.G.; project administration, J.W.A.; resources, J.W.A.; software, B.F.; supervision, T.F. and J.W.A.; validation, S.G., B.F., and J.W.A.; visualization, B.F.; writing—original draft, S.G.; writing—review and editing, T.F.

Funding: This research was supported by the National Strategic Project-Carbon Mineralization Flagship Center of the National Research Foundation of Korea (NRF) funded by the Ministry of Science and ICT (MSIT), the Ministry of Environment (ME) and the Ministry of Trade, Industry and Energy (MOTIE). (2017M3D8A2084752).

Conflicts of Interest: The authors declare no conflict of interest. The funders had no role in the design of the study; in the collection, analyses, or interpretation of data; in the writing of the manuscript, or in the decision to publish the results.

References

1. Bode, H. *Lead-Acid Batteries*; U.S. DOE: Washington, DC, USA, 1977; pp. 1–15.
2. Bhangu, B.S.; Bentley, P.; Stone, D.A.; Bingham, C.M. Nonlinear observers for predicting state-of-charge and state-of-health of lead-acid batteries for hybrid-electric vehicles. *IEEE Trans. Veh. Technol.* **2005**, *54*, 783–794. [CrossRef]
3. Parker, C.D. Lead–acid battery energy-storage systems for electricity supply networks. *J. Power Sources* **2001**, *100*, 18–28. [CrossRef]
4. Zou, G.; Dou, Y.; Chang, X.; Chen, Y. Design and application of a standalone hybrid wind-solar system for automatic observation systems used in the polar region. *Appl. Sci.* **2018**, *8*, 2376.
5. Chang, Y.; Mao, X.; Zhao, Y.; Feng, S.; Chen, H.; Finlow, D. Lead-acid battery use in the development of renewable energy systems in China. *J. Power Sources* **2009**, *191*, 176–183. [CrossRef]
6. Pavlov, D. *Lead-Acid Batteries: Science and Technology*, 1st ed.; Elsevier Science: Oxford, UK, 2011; pp. 21–26.
7. Recycling Used Lead-Acid Batteries: Health Considerations. Available online: https://apps.who.int/iris/bitstream/handle/10665/ (accessed on 31 May 2019).
8. Sun, Z.; Cao, H.; Zhang, X.; Lin, X.; Zheng, W.; Cao, G.; Sun, Y.; Zhang, Y. Spent lead-acid battery recycling in China–A review and sustainable analyses on mass flow of lead. *Waste Manag.* **2017**, *64*, 190–201. [CrossRef] [PubMed]
9. Ellis, T.W.; Mirza, A.H. The refining of secondary lead for use in advanced lead-acid batteries. *J. Power Sources* **2010**, *195*, 4525–4529. [CrossRef]
10. Bernardes, A.M.; Espinosa, D.C.R.; Tenorio, J.A.S. Recycling of batteries: A review of current processes and technologies. *J. Power Sources* **2004**, *130*, 291–298. [CrossRef]
11. Zhu, X.; Yang, J.; Gao, L.; Liu, J.; Yang, D.; Sun, X.; Zhang, W.; Wang, Q.; Li, L.; He, D.; et al. Preparation of lead carbonate from spent lead paste via chemical conversion. *Hydrometallurgy* **2013**, *134–135*, 47–53. [CrossRef]
12. Andrews, D.; Raychaudhuri, A.; Frias, C. Environmentally sound technologies for recycling secondary lead. *J. Power Sources* **2000**, *88*, 124–129. [CrossRef]

13. Liu, W.; Tian, J.; Chen, L.; Guo, Y. Temporal and spatial characteristics of lead emissions from the lead-acid battery manufacturing industry in China. *Environ. Pollut.* **2017**, *220*, 696–703. [CrossRef]
14. Spanos, C.; Berlinger, S.A.; Jayan, A.; West, A.C. Inverse Charging Techniques for Sulfation Reversal in Flooded Lead-Acid Batteries. *J. Electrochem. Soc.* **2016**, *163*, A1612–A1618. [CrossRef]
15. Jolly, R.; Rhin, C. The recycling of lead-acid batteries: Production of lead and polypropylene. *Resour. Conserv. Recycl.* **1994**, *10*, 137–143. [CrossRef]
16. Rust, N.; Ferg, E.E.; Masalova, I. A degradation study of isotactic virgin and recycled polypropylene used in lead acid battery casings. *Polym. Test.* **2006**, *25*, 130–139. [CrossRef]
17. Hong, S.; Cannon, F.S.; Hou, P.; Byrne, T.; Nieto-Delgado, C. Adsorptive removal of sulfate from acid mine drainage by polypyrrole modified activated carbons: Effects of polypyrrole deposition protocols and activated carbon source. *Chemosphere* **2017**, *184*, 429–437. [CrossRef] [PubMed]
18. Cuesta Mayorga, I.; Astilleros, J.M.; Fernández-Díaz, L. Precipitation of $CaCO_3$ polymorphs from aqueous solutions: The role of pH and sulfate groups. *Minerals* **2019**, *9*, 178. [CrossRef]
19. Gominsek, T.; Lubej, A.; Pohar, C. Continuous precipitation of calcium sulfate dehydrate from waste sulfuric acid and lime. *J. Chem. Technol. Biotechnol.* **2005**, *80*, 939–947. [CrossRef]
20. Najib, T.; Solgi, M.; Farazmand, A.; Heydarian, S.M.; Nasernejad, B. Optimization of sulfate removal by sulfate reducing bacteria using response surface methodology and heavy metal removal in a sulfidogenic UASB reactor. *J. Environ. Chem. Eng.* **2017**, *5*, 3256–3265. [CrossRef]
21. Arahman, N.; Mulyati, S.; Lubis, M.R.; Takagi, R.; Matsuyama, H. Removal profile of sulfate ion from mix ion solution with different type and configuration of anion exchange membrane in electrodialysis. *J. Water Process Eng.* **2017**, *20*, 173–179. [CrossRef]
22. Kartic, D.N.; Narayana, B.C.H.A.; Arivazhagan, M. Removal of high concentration of sulfate from pigment industry effluent by chemical precipitation using barium chloride: RSM and ANN modeling approach. *J. Environ. Manag.* **2018**, *206*, 69–76. [CrossRef]
23. Fang, P.; Tang, Z.; Chen, X.; Huang, J.; Tang, Z.; Cen, C. Removal of High-Concentration Sulfate Ions from the Sodium Alkali FGD Wastewater Using Ettringite Precipitation Method: Factor Assessment, Feasibility, and Prospect. *J. Chem.* **2018**, *2018*, 1265168. [CrossRef]
24. Garrels, R.M.; Thompson, M.E. A chemical model for sea water at 25 degrees C and one atmosphere total pressure. *Am. J. Sci.* **1962**, *260*, 57–66. [CrossRef]
25. Helgeson, H.C.; Kirkham, D.H.; Flowers, G.C. Theoretical prediction of the thermodynamic behavior of aqueous electrolytes by high pressures and temperatures; IV, Calculation of activity coefficients, osmotic coefficients, and apparent molal and standard and relative partial molal properties to 600 degrees C and 5kb. *Am. J. Sci.* **1981**, *281*, 1249–1516.
26. Oelkers, E.H.; Helgeson, H.C. Triple-ion anions and polynuclear complexing in supercritical electrolyte solutions. *Geochim. Cosmochim. Acta* **1990**, *54*, 727–738. [CrossRef]
27. Shock, E.L.; Oelkers, E.H.; Johnson, J.W.; Sverjensky, D.A.; Helgeson, H.C. Calculation of the thermodynamic properties of aqueous species at high pressures and temperatures. Effective electrostatic radii, dissociation constants and standard partial molal properties to 1000 °C and 5 kbar. *J. Chem. Soc. Faraday Trans.* **1992**, *88*, 803–826. [CrossRef]
28. Karimi, H. Effect of pH and initial Pb(II) concentration on the lead removal efficiency from industrial wastewater using $Ca(OH)_2$. *Int. J. Water Wastewater Treat.* **2017**, *3*, 1–4.